

# An asymmetric supercapacitor based on a NiO/Co<sub>3</sub>O<sub>4</sub>@NiCo cathode and an activated carbon anode

Jing Li <sup>1</sup>, Pei-chao Zou <sup>1</sup>, Wen-tao Yao <sup>1</sup>, Peng Liu <sup>1</sup>, Fei-yu Kang <sup>1,2</sup>, Cheng Yang <sup>1,\*</sup>

<sup>1</sup>Division of Energy and Environment, Shenzhen International Graduate School, Tsinghua University, Shenzhen 518055, China;

<sup>2</sup>School of Materials Science and Engineering, Tsinghua University, Beijing 100084, China

**Abstract:** Pseudocapacitive metal oxide active materials are promising for use in high performance supercapacitors. However, their poor electrical conductivity greatly hinders their practical application. We formed NiO and Co<sub>3</sub>O<sub>4</sub> active materials on the surface of a highly conductive NiCo nanowire membrane current collector by a simple air oxidation method to fabricate a self-supported flexible NiO/Co<sub>3</sub>O<sub>4</sub>@NiCo electrode. This significantly improves electron transport at the interface between the current collector and the active NiO/Co<sub>3</sub>O<sub>4</sub>. Furthermore, the reticular nanowire network facilitates ion transportation and releases strain caused during charge and discharge. Due to this unique structural characteristic, the NiO/Co<sub>3</sub>O<sub>4</sub>@NiCo electrode delivers a high specific capacitance of 1.36 F cm<sup>-2</sup> at a current density of 5 mA cm<sup>-2</sup>, and excellent cycling stability with a capacitance retention of 96.95% after 10 000 cycles. An asymmetric supercapacitor was assembled using the NiO/Co<sub>3</sub>O<sub>4</sub>@NiCo as the cathode and an activated carbon electrode as the anode, which delivered an energy density of 0.32 mWh cm<sup>-2</sup> at a power density of 8 mW cm<sup>-2</sup>. Even at a high power density of 40 mW cm<sup>-2</sup>, an energy density of 0.17 mWh cm<sup>-2</sup> was achieved, suggesting its promising use as an efficient electrode for high performance supercapacitors.

**Key Words:** Nickel oxide; Cobalt oxide; Activated carbon; Integrated electrode; Asymmetric supercapacitor

## 1 Introduction

Electrochemical energy storage (EES) devices have attracted considerable interest in various fields over the last few decades<sup>[1]</sup>. Supercapacitors (SCs) are one of the most promising candidates for EES devices, which have drawn much attention owing to their high power density, fast charging rate and long cycle life<sup>[2]</sup>. Based on the type of energy storage mechanisms, supercapacitors can be classified into electrical double layer capacitors (EDLCs) and pseudocapacitors. In EDLCs, the energy storage is based on the adsorption of electrolyte ions on the surface of electrodes. Carbon-based materials<sup>[3-4]</sup> are widely used in EDLC electrodes owing to their large surface area and good electrochemical stability. While for the pseudocapacitors, the energy storage ability comes from the reversible faradaic redox reactions occurring at the interface between the electrolyte and the electroactive materials<sup>[5]</sup>. The active materials for pseudocapacitors include transition metal oxides/hydroxides (e.g. the MnO<sub>2</sub><sup>[6]</sup>, Co<sub>3</sub>O<sub>4</sub><sup>[7]</sup>, MoO<sub>3</sub><sup>[8]</sup>, Ni(OH)<sub>2</sub><sup>[9]</sup>), transition metal sulfides (e.g. MoS<sub>2</sub><sup>[10]</sup>), and conducting polymers (e.g. polyaniline<sup>[11]</sup> and polypyrrole<sup>[12]</sup>), etc. The high redox activities, high theoretical capacities and great reversibility make the pseudocapacitive materials promising electrode materials in supercapacitors<sup>[13-14]</sup>. However, the rate capability and cycle stability of

pseudocapacitive materials such as NiO and Co<sub>3</sub>O<sub>4</sub>, are usually inferior to others due to their limited electronic conductivity<sup>[9, 15-16]</sup>. Intensive efforts have been made to solve the problem of poor conductivity of the metal oxides. For instance, the widely used slurry coating method, involving conductive additives and binders is effective to improve the conductivity of the electrode. But the introduction of non-active materials inevitably compromises the electron/ion transport<sup>[17]</sup>. Another way is to combine active material with various kinds of large surface area porous current collectors<sup>[18]</sup> (e.g. carbon cloth, nickel foam, graphene, etc) using multiple methods such as vacuum filtration<sup>[19]</sup>, hydrothermal<sup>[20]</sup>, and electrodeposition.<sup>[21]</sup> The porous current collectors can improve the ion transport to enhance electrode performance, and the large surface area with abundant electroactive sites can facilitate the rapid Faradic redox reactions, but the contact resistance between the current collectors and the active materials still needs to be improved<sup>[22]</sup>. Therefore, fabricating self-supported electrode without additives and in-situ formed active material on the high surface area, conductive and porous electrode is a promising approach to improve the electrical conductivity, charge transport efficiency and overall electrochemical performance<sup>[23]</sup>.

In this work, we utilize NiCo nanowire membrane<sup>[24]</sup> as

Received date: 25 Jan. 2020; Revised date: 18 Mar. 2020

\*Corresponding author. E-mail: Yang.Cheng@sz.tsinghua.edu.cn

Copyright©2020, Institute of Coal Chemistry, Chinese Academy of Sciences. Published by Elsevier Limited. All rights reserved.

DOI: 10.1016/S1872-5805(20)60478-4

the current collector for its high conductivity and in-situ prepared NiO/Co<sub>3</sub>O<sub>4</sub> active material by a facile oxidation method. The in-situ formed active material on the conductive nanowire network can significantly improve the electron transport ability between the current collector and the active material. Furthermore, the reticular nanowire network structure can facilitate the ion transportation and release the strain generated during the charge and discharge process. As a result, the integrated electrode delivered a high specific capacitance of 1.36 F cm<sup>-2</sup> at a current density of 5 mA cm<sup>-2</sup>, and was steadily cycled for 10,000 cycles with a capacitance retention of 96.95%. Furthermore, the asymmetric supercapacitor consisting of the NiO/Co<sub>3</sub>O<sub>4</sub>@NiCo positive electrode and activated carbon negative electrode can deliver an energy density of 0.32 mWh cm<sup>-2</sup> at a power density of 8 mW cm<sup>-2</sup>. Even at a high power density of 40 mW cm<sup>-2</sup>, an energy density of 0.17 mWh cm<sup>-2</sup> was maintained. Moreover, the asymmetric supercapacitor can be steadily cycled for 5000 cycles with a capacitance retention of 95.12%.

## 2 Experimental

### 2.1 Fabrication of the NiCo nanowire membrane current collector

The NiCo nanowire membrane was fabricated using a modified template-free method<sup>[24]</sup>. Aqueous solution A contained 0.03 mol/L Na<sub>3</sub>C<sub>6</sub>H<sub>5</sub>O<sub>7</sub>·2H<sub>2</sub>O, 0.05 mol/L NiCl<sub>2</sub>·6H<sub>2</sub>O, 0.05 mol/L CoCl<sub>2</sub>·6H<sub>2</sub>O and 0.20 mmol/L H<sub>2</sub>PtCl<sub>6</sub>·6H<sub>2</sub>O, and aqueous solution B contained 8% of N<sub>2</sub>H<sub>4</sub>·H<sub>2</sub>O. Using the 6 mol/L KOH aqueous solution, the pH values of solution A and solution B were adjusted to 12.5 at room temperature. After 20 mL solution A and 20 mL solution B were preheated to 80 °C in the water bath, they were mixed together with a glass rod in a 100 ml beaker and placed in the water bath with a piece of magnet on the beaker. The temperature of the water bath was maintained at 80 °C. After reaction for 6 min, the beaker was moved out of the water bath. The black membrane can be obtained and was washed with deionized water and ethanol, and then compressed to a mat using a glass rod.

### 2.2 Fabrication of the NiO/Co<sub>3</sub>O<sub>4</sub>@NiCo nanowire electrode

The NiO/Co<sub>3</sub>O<sub>4</sub>@NiCo electrode was synthesized through an in-situ oxidation method. The as-prepared NiCo nanowire membranes were annealed in a muffle furnace at 250 °C (5 °C /min) in air for 1, 5, 10 and 15 h to obtain the Co<sub>3</sub>O<sub>4</sub> and NiO metal oxides.

### 2.3 Materials characterization

The crystallographic information of the samples with different oxidation times was characterized by X-ray diffraction (XRD) (BrukerDS RINT2000/PC, Germany). The morphology of the NiCo current collectors and NiO/Co<sub>3</sub>O<sub>4</sub>@NiCo electrodes were characterized by Field

Emission Scanning Electron Microscopy (FE-SEM, SAPHIRE SUPRA 55) and Transmission Electron Microscopy (TEM, FEI-G2 Spirit, Germany, working voltage 300 kV). X-ray photoelectron spectroscopy (XPS) was conducted using a X-ray photon-electron spectrometer (XPS, PHI 5000 VersaProbe II).

### 2.4 Fabrication of activated carbon electrode

The commercial activated carbon, acetylene black and PVDF was mixed with a mass ratio of 8:1:1 in N-Methyl pyrrolidone (NMP) and then dispensed on Ti foil to prepare the activated carbon electrode.

### 2.5 Electrochemical measurement

The cyclic voltammetry (CV) and galvanostatic charge-discharge (GCD) behaviours of pristine NiCo current collector and the as-prepared NiO/Co<sub>3</sub>O<sub>4</sub>@NiCo electrode were investigated using an electrochemical station (VMP3, Bio-Logic, France) by a three-electrode configuration in a 1 mol/L KOH aqueous electrolyte at room temperature. Pt and Hg/HgO electrode were employed as the counter and reference electrodes, respectively. During the electrochemical measurement, the applied potential window was set from 0 V to 0.5 V.

The specific areal capacitances of the samples were calculated from GCD curves according to the following equation:

$$C = \frac{I \cdot \Delta t}{V \cdot \Delta U}$$

Where  $I$  is the current density,  $\Delta t$  is the discharge time,  $V$  is the area of the positive and negative materials,  $\Delta U$  is the potential range, and  $C$  is the specific areal capacitance. The calculation of the energy density ( $E$ ) and power density ( $P$ ) is based on the equations below:

$$E = \frac{C \Delta U^2}{2}$$

$$P = \frac{E}{\Delta t}$$

Where  $C$  is the specific areal capacitance of the asymmetric supercapacitor,  $\Delta U$  is the potential window of the discharge process, and  $\Delta t$  is the discharge time.

The Electrochemical Impedance Spectroscopy (EIS) measurements were conducted in the frequency range between 100 KHz and 10 mHz with an amplitude of 5 mV.

## 3 Results and discussion

The fabrication of the self-supported NiCo nanowire membrane was realized by the modified method reported previously (Fig. 1a)<sup>[24-25]</sup>. The NiO/Co<sub>3</sub>O<sub>4</sub>@NiCo electrode was obtained simply by annealing the NiCo nanowire at 250°C in air to in-situ convert the surface Ni and Co into NiO and Co<sub>3</sub>O<sub>4</sub>, respectively.

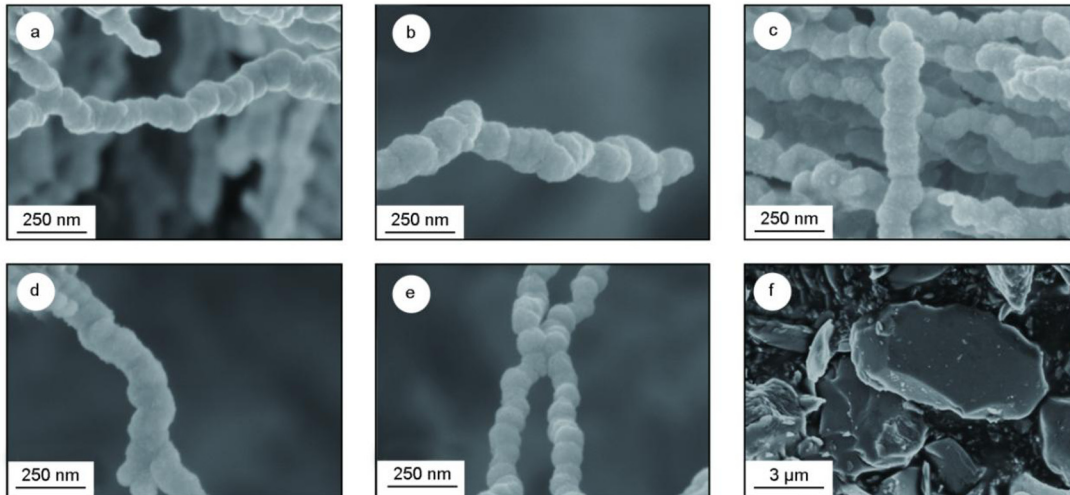


Fig. 1 (a-e) SEM images of NiCo nanowire with different oxidation times: (a) NiCo-0 h, (b) NiCo-1 h, (c) NiCo-5 h, (d) NiCo-10 h, (e) NiCo-15 h and (f) activated carbon.

Herein, the samples obtained after annealing for 1, 5, 10 and 15 h were denoted as NiCo-1 h, NiCo-5 h, NiCo-10 h and NiCo-15 h, respectively. As shown in Fig. 1b-e, after annealing at 250 °C, the structure of the nanowire remained stable with increasing the oxidation time from 1 to 15 h, indicating that the NiCo nanowire was robust enough to endure the oxidation in air without severe destruction. The particle morphology of the activated carbon is shown in Fig. 1f.

The crystallinity information of the samples can be obtained from XRD. Fig. 2a shows the XRD patterns of NiCo-0 h, NiCo-1 h, NiCo-5 h, NiCo-10 h and NiCo-15 h samples. For the NiCo-0 h sample, the diffraction peaks located at 47.6°, 75.9°, 44.8° can be indexed to (101), (110), (002) planes of hexagonal Co (JCPDS No.05-0727), respectively. The peak positions of (111), (200) and (220) planes for fcc Ni shifted, which could be attributed to the lattice distortion from the partially formation of fcc NiCo alloy phase according to our previous study<sup>[24]</sup>. After oxidized for a series of times, the diffraction peaks located at 43.3°, 37.3°, 62.9° can be indexed to (200), (111), (220) planes of NiO (JCPDS No.04-0835), while the peaks located at 36.9°,

65.2°, 59.3° can be indexed to (311), (440), (511) planes of Co<sub>3</sub>O<sub>4</sub>, respectively (JCPDS No.42-1467)<sup>[26]</sup>. Magnified patterns of the selected areas from 2θ= 55°-68° are given in Fig. 2b, the weak XRD peaks of NiO might arise from the relatively weak crystallization of NiO composed with an amorphous phase<sup>[27]</sup>. Fig. S1 shows the XRD pattern of the activated carbon, which shows broad peaks at 23° and 45°, indicating the amorphous phase<sup>[28]</sup>.

To investigate the morphology and structure of the NiO/Co<sub>3</sub>O<sub>4</sub>@NiCo sample, the transmission electron microscopy (TEM) image of the NiCo-10 h sample were conducted. As shown in Fig. 3a, the TEM image of the NiCo-10 h shows that the the NiO/Co<sub>3</sub>O<sub>4</sub>@NiCo nanowire has a diameter of less than 200 nm. Fig. 3b shows the HRTEM image of the NiO/Co<sub>3</sub>O<sub>4</sub>@NiCo sample on the edge part. The lattice fringe with a space of 0.243 nm corresponds to the (311) plane of Co<sub>3</sub>O<sub>4</sub>, while the lattice fringe with a space of 0.209 nm corresponds to the (200) plane of NiO. The Ni, Co and O elements were found to be evenly distributed within the nanowire via energy dispersive spectroscopy (EDS) mapping (Fig. 3c-f).

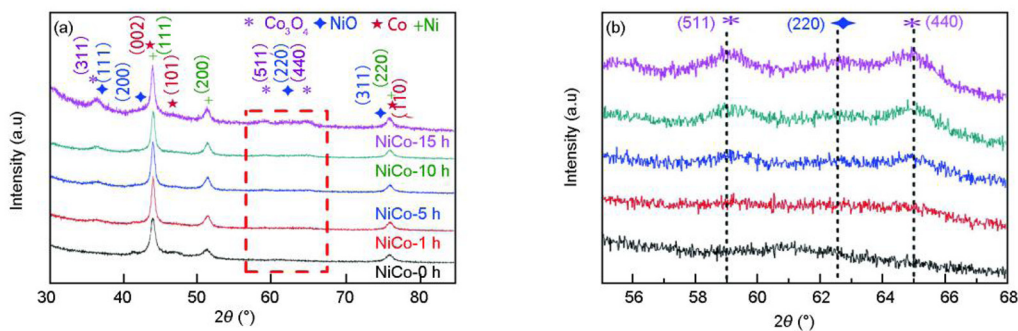


Fig. 2 XRD patterns of (a) NiCo-0 h, NiCo-1 h, NiCo-5 h, NiCo-10 h and NiCo-15 h and (b) magnified patterns of selected areas from 2θ= 55°-68°.

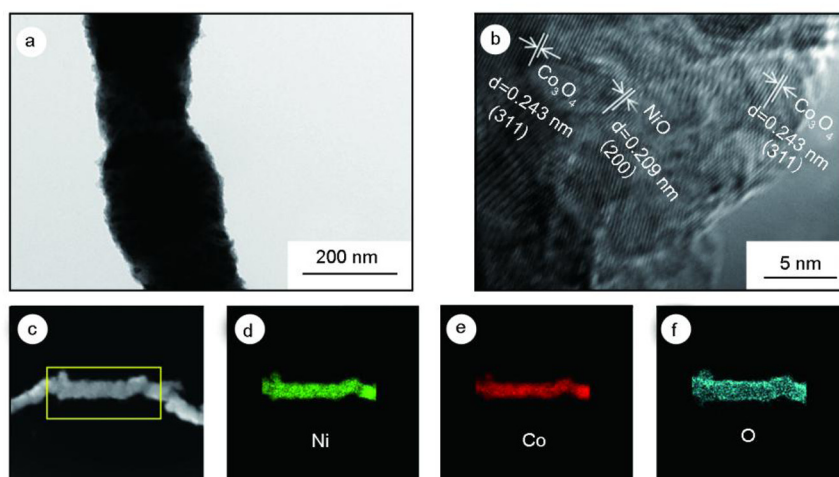


Fig. 3 (a) TEM, (b) HRTEM and (c-f) EDS mapping images of the NiO/Co<sub>3</sub>O<sub>4</sub>@NiCo sample (NiCo-10 h).

The chemical composition of the NiO/Co<sub>3</sub>O<sub>4</sub>@NiCo electrode was further characterized using X-ray photoelectron spectroscopy (XPS). The full XPS spectrum of the NiCo-10 h sample is shown in Fig. 4a, which can demonstrate the existence of Ni, Co and O elements in the NiO/Co<sub>3</sub>O<sub>4</sub>@NiCo electrode. The O 1s spectrum is shown in Fig 4b and the two peaks at the binding energy of 527.64 and 529.46 eV were due to the oxygen in hydroxyl group and metal-oxygen bonds respectively. Fig. 4c displays the spectrum of Ni 2p. The Ni 2p<sub>1/2</sub> and Ni 2p<sub>3/2</sub> peaks exhibited a pair of spin-orbit doublets at 871.25 and 853.39 eV, respectively. Another two peaks

located at 859.50 and 878.37 eV assigned their respective shake-up satellite peaks (denoted as Sat.), which are characteristics of Ni<sup>2+</sup> [24]. Similarly, the fine-scanned Co 2p spectrum can be deconvoluted into a pair of spin-orbit doublets, as shown in Fig. 4d. The peaks located at 777.75, 793.21, 779.02 and 794.48 eV were attributed to Co<sup>3+</sup> 2p<sub>3/2</sub>, Co<sup>3+</sup> 2p<sub>1/2</sub>, Co<sup>2+</sup> 2p<sub>3/2</sub> and Co<sup>2+</sup> 2p<sub>1/2</sub> peaks, respectively. Two satellite peaks were observed at 785.30 eV (Co 2p<sub>3/2</sub>) and 802.42 eV (Co 2p<sub>1/2</sub>). The Co 2p spectrum further confirmed the existence of Co<sub>3</sub>O<sub>4</sub> in the sample<sup>[7]</sup>.

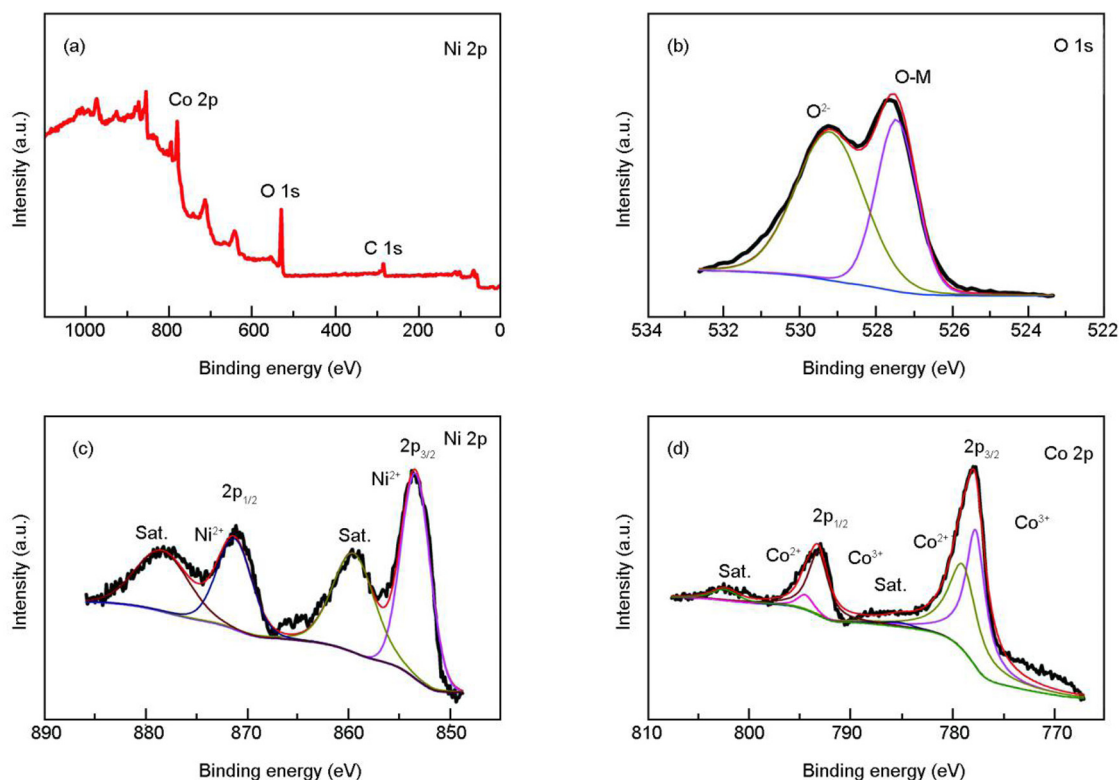


Fig. 4. (a) Full XPS spectrum, (b) O 1s spectrum, (c) Ni 2p spectrum and (d) Co 2p spectrum of the NiO/Co<sub>3</sub>O<sub>4</sub>@NiCo sample (NiCo-10 h).

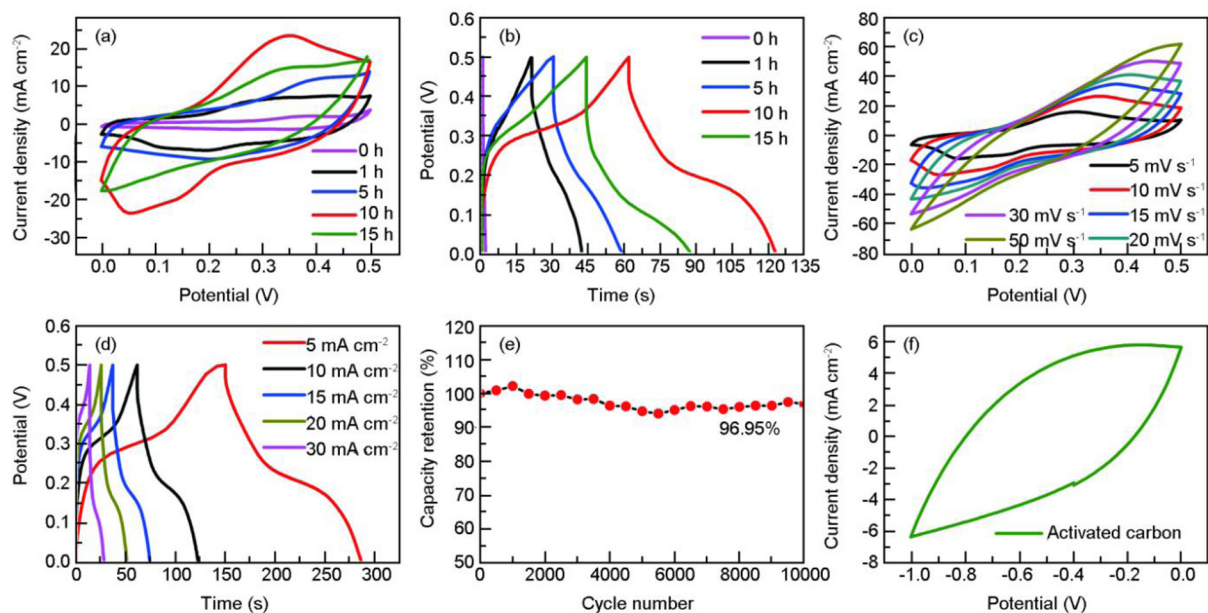
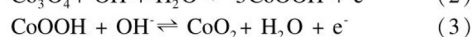
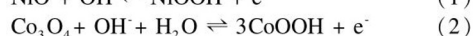
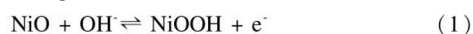


Fig. 5. (a) CV curves of the NiCo membrane with different oxidation times, (b) GCD curves of the NiCo membrane with different oxidation times, (c) CV curves of the NiO/Co<sub>3</sub>O<sub>4</sub>@NiCo electrode with different scan rates, (d) GCD curves of the NiO/Co<sub>3</sub>O<sub>4</sub>@NiCo electrode at different current densities, (e) cycle stability of the NiCo-10 h electrode and (f) CV curve of the activated carbon.

To explore the electrochemical performance of the composite electrode, CV and GCD were conducted in a three-electrode configuration using as-prepared samples as the working electrode, 1M KOH aqueous solution as the electrolyte, a platinum foil as the counter electrode and a Hg/HgO electrode as the reference electrode. Fig. 5a shows the CV curves of the electrode with different oxidation times (NiCo-0 h, NiCo-1 h, NiCo-5 h, NiCo-10 h, NiCo-15 h) at a scan rate of 10 mV s<sup>-1</sup>. The NiCo-10 h curve showed a larger enclosed area than the other samples, indicating that NiCo-10 h had the highest specific areal capacitance. Fig. 5b shows the GCD curves of the electrodes with different oxidation times at the current density of 10 mA cm<sup>-2</sup>. The NiCo-10 h electrode exhibited the highest charge-discharge time compared to the other samples, which is in accordance with the CV curves. The areal capacitance of the samples were estimated based on the discharge times and the measured values were 0.396 F cm<sup>-2</sup> for NiCo-1 h, 0.57 F cm<sup>-2</sup> for NiCo-5 h, 1.25 F cm<sup>-2</sup> for NiCo-10 h and 0.989 F cm<sup>-2</sup> for NiCo-15 h. Therefore, we considered the NiCo-10 h an optimum sample and further examined the electrochemical properties. The amount of active material in the NiCo-10 h electrode is estimated in the range of 2.91-3.61 mg cm<sup>-2</sup> (Details shown in the supporting information). Fig. 5c displays the CV curves of the NiCo-10 h electrode at various scan rates ranging from 5 to 50 mV s<sup>-1</sup>. The couple of redox peaks observed in each CV curve indicated the existence of reversible Faradaic redox process in the electrode. The redox reactions of the NiO/Co<sub>3</sub>O<sub>4</sub>@NiCo electrode are given as below<sup>[29]</sup>:



The CV curves represented an excellent reversible behavior under increased scan rates, suggesting the lower contact resistance and fast electron/ion transport. The GCD curves at different current densities ranging from 5 to 30 mA cm<sup>-2</sup> were also measured to estimate the capacitance behavior and rate capability of the material as shown in Fig. 5d. The quasi-triangular shape with a plateau at about 0.15 to 0.25 V confirmed the pseudocapacitance of the electrode. The areal capacitance of the NiCo-10 h electrode was measured to be 1.36, 1.24, 1.11, 1 and 0.84 F cm<sup>-2</sup> at the current density of 5, 10, 15, 20 and 30 mA cm<sup>-2</sup>, respectively, showing a good rate capability (as shown in Fig S2). Fig. 5e shows the cycling stability of the electrode at a scan rate of 30 mV s<sup>-1</sup>, the electrode showed a capacitance retention of 96.95% after 10 000 cycles. The superior performance of the NiO/Co<sub>3</sub>O<sub>4</sub>@NiCo electrode is due to the sufficient and large surface area active materials and the high conductivity of the NiCo current collector, facilitating the access of electrolyte ions to the electrode surface, and improving the electron transport efficiency. Fig. 5f shows the CV curve of the activated carbon at a scan rate of 10 mV s<sup>-1</sup>, and the specific capacitance was measured to be 193.5 mF cm<sup>-2</sup>.

The NiCo-10 h electrode exhibited the best electrochemical performance among all the samples, which can be attributed to a trade-off between the loading amount of active material and electronic conductance of the electrode. With the increase of the oxidation time, the amount of the active material increases (as shown in Fig. S3). However, the conductivity of the electrode is reduced due to the increased amount of the metal oxides (Fig. S4). The prolonging the oxidation time increased the amount of active materials but reduced the conductivity of the electrode. The active material

thus cannot be fully utilized due to the less conductive current collector. With a moderate amount of active material and an appropriate conductivity, the electrode oxidized for 10 h, therefore, exhibited the best electrochemical performance.

To evaluate the performance of the NiO/Co<sub>3</sub>O<sub>4</sub>@NiCo electrode at the device level, asymmetric supercapacitors were assembled by employing the NiO/Co<sub>3</sub>O<sub>4</sub>@NiCo electrode as the positive electrode, the activated carbon as the negative electrode, 1 M KOH aqueous solution as the electrolyte and glass fiber as the separator. As shown in Fig. 6a, a series of CV tests in different potential regions were conducted at a scan rate of 10 mV s<sup>-1</sup>, suggesting that the potential window of the device could be expected to be 1.6 V. As shown in Fig. 6b, the well maintained CV curves of the asymmetric supercapacitor explored at different scan rates ranging from 5-100 mV s<sup>-1</sup> demonstrated the good reversibility of the asymmetric supercapacitor. Fig. 6c shows the GCD curves of the asymmetric supercapacitor at different current densities from 10 to 50 mA cm<sup>-2</sup>. The calculated areal capacitance of the asymmetric supercapacitor was 0.90, 0.82, 0.74, 0.64 and 0.47 F cm<sup>-2</sup> at the current densities of 10, 15, 20, 30 and 50 mA cm<sup>-2</sup>, respectively. Fig. 6d shows the cycling stability of the asymmetric supercapacitor at a scan rate of 30 mV s<sup>-1</sup>. The asymmetric supercapacitor was stably cycled for 5 000 cycles with a capacitance retention of 95.12%, revealing its remarkable cycling stability. The EIS measurement of the

asymmetric supercapacitor is shown in Fig. 6e, the simulated Re/Rct of the asymmetric supercapacitor before and after cycles were 1.413 Ω/1.339 Ω and 1.359 Ω/1.238 Ω, respectively, indicating the low contact resistance and excellent charge transfer ability of the asymmetric supercapacitor. Moreover, at the current density of 10 mA cm<sup>-2</sup>, the asymmetric supercapacitor delivered a high energy density of 0.32 mWh cm<sup>-2</sup> with a power density of 8 mW cm<sup>-2</sup>. Even at a high power density of 40 mW cm<sup>-2</sup>, an energy density of 0.17 mWh cm<sup>-2</sup> was still maintained. Fig. 6f shows the Ragone plot of the asymmetric supercapacitor, and the performance was superior or comparable to many reported asymmetric/hybrid supercapacitors such as the Cu<sub>2</sub>O/Cu/GCP//CP<sup>[30]</sup>, CC@CuHCF-3//AC<sup>[31]</sup>, NSA@CO<sub>3</sub>O<sub>4</sub>-NiO//AC<sup>[7]</sup>, and PPy/RGO/CNT/BC<sub>20</sub> supercapacitors<sup>[32]</sup>.

The excellent performance of the asymmetric supercapacitor can be assigned to the structure design of the electrode. Using the simple in-situ oxidation method, the active material NiO/Co<sub>3</sub>O<sub>4</sub> were in-situ formed on the surface of the high conductivity NiCo current collector, rendering low contact resistance between the current collector and the metal oxides. The large surface area of the nanowire can provide sufficient electrochemical active sites and facilitate the ion transportation. Furthermore, the stable nanowire can release stress during redox reactions, thus improving the performance of the integrated electrode.

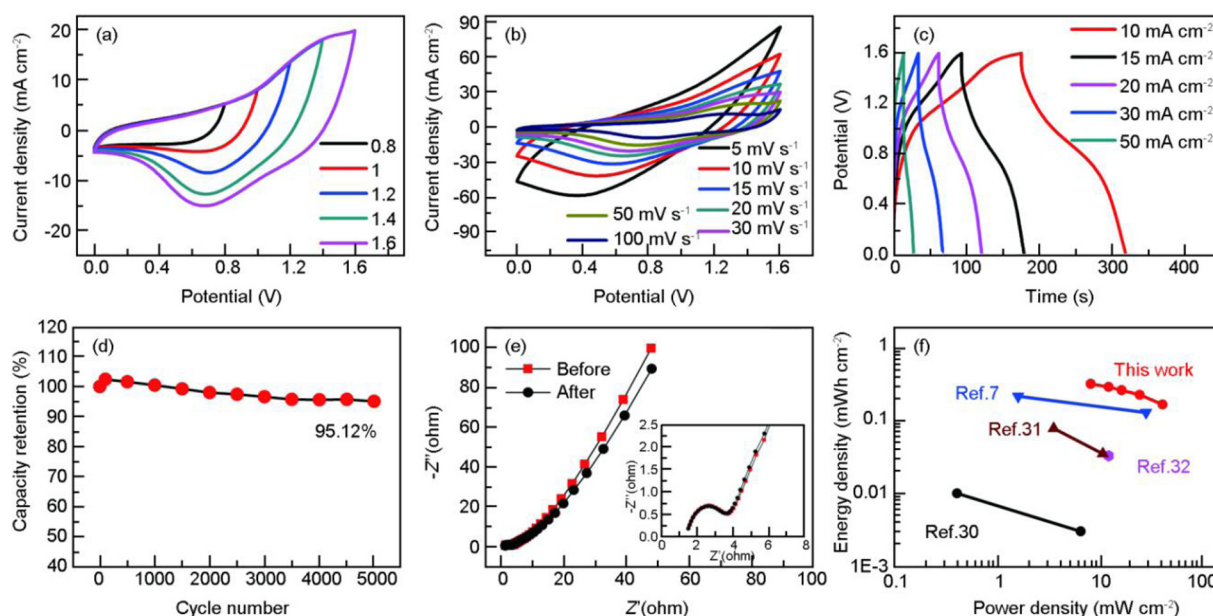


Fig. 6. (a) CV curves of the asymmetric supercapacitor measured in the different potential regions, (b) CV curves of the asymmetric supercapacitor measured at different scan rates, (c) GCD curves of the asymmetric supercapacitor measured at different current densities, (d) Cycle stability of the NiO/Co<sub>3</sub>O<sub>4</sub>@NiCo//AC asymmetric supercapacitor, (e) Nyquist plots of the NiO/Co<sub>3</sub>O<sub>4</sub>@NiCo//AC asymmetric supercapacitor before and after cycles, the inset showing the Nyquist plot in high-frequency and (f) Ragone plots of the NiO/Co<sub>3</sub>O<sub>4</sub>@NiCo//AC asymmetric supercapacitors.

## 4 Conclusions and outlook

In summary, we have fabricated the self-supported NiO/Co<sub>3</sub>O<sub>4</sub>@NiCo integrated electrodes by a facile in-situ oxidation method. The integrated electrode exhibited a high areal capacitance of 1.36 F cm<sup>-2</sup> at a current density of 5 mA cm<sup>-2</sup> and a high cycle stability with a capacitance retention of 96.95% after 10 000 cycles. The asymmetric supercapacitor consisting of the NiO/Co<sub>3</sub>O<sub>4</sub>@NiCo cathode electrode coupled with the activated carbon anode can deliver a high energy density of 0.32 mWh cm<sup>-2</sup> at a power density of 8 mW cm<sup>-2</sup>. Even at a high power density of 40 mWcm<sup>-2</sup>, an energy density of 0.17 mWh cm<sup>-2</sup> was achieved. The excellent performance of the integrated electrode could be attributed to the high conductivity NiCo current collector and the in-situ formed NiO/Co<sub>3</sub>O<sub>4</sub> active materials, which can largely decrease the contact resistance and sufficiently improve the electron transport efficiency. Furthermore, the reticular nanowire network structure can also improve the transport of ions and release the strain caused during charge and discharge process.

Besides in-situ oxidation, other types of active materials can also be fabricated by e.g. nitridation, phosphorization and sulfidation, which may show even better performance, and can be further explored in future works. We expect that our current study can inspire future development of electrode materials and energy storage systems.

## Acknowledgements

The authors thank the Local Innovative and Research Teams Project of Guangdong Pearl River Talents Program (2017BT01N111), Shenzhen Geim Graphene Center, the National Nature Science Foundation of China (Project No. 51578310), Guangdong Province Science and Technology Department (Project No. 2015A030306010), and Shenzhen Government (Project No. JCYJ20170412171720306) for financial supports.

## Supporting Information

Supplementary data associated with this article can be found in the online version.

## References

- [1] Ortabay S, Alper J P, Rossi F, et al. MnO<sub>x</sub>-decorated carbonized porous silicon nanowire electrodes for high performance supercapacitors [J]. *Energy & Environmental Science*, 2017, 10 (6): 1505-1516.
- [2] Xu C, Li Z, Yang C, et al. An ultralong, highly oriented nickel-nanowire-array electrode scaffold for high-performance compressible pseudocapacitors [J]. *Advanced Materials*, 2016, 28 (21): 4105-10.
- [3] Zang X, Zhang R, Zhen Z, et al. Flexible, temperature-tolerant supercapacitor based on hybrid carbon film electrodes [J]. *Nano Energy*, 2017, 40: 224-232.
- [4] Xie B, Wang Y, Lai W, et al. Laser-processed graphene based micro-supercapacitors for ultrathin, rollable, compact and designable energy storage components [J]. *Nano Energy*, 2016, 26: 276-285.
- [5] Wang F, Wu X, Yuan X, et al. Latest advances in supercapacitors: from new electrode materials to novel device designs [J]. *Chemical Society Reviews*, 2017, 46 (22): 6816-6854.
- [6] Wang Y, Lai W, Wang N, et al. A reduced graphene oxide/mixed-valence manganese oxide composite electrode for tailorable and surface mountable supercapacitors with high capacitance and super-long life [J]. *Energy & Environmental Science*, 2017, 10 (4): 941-949.
- [7] Chandra Sekhar S, Nagaraju G, Yu J S. High-performance pouch-type hybrid supercapacitor based on hierarchical NiO-Co<sub>3</sub>O<sub>4</sub>-NiO composite nanoarchitectures as an advanced electrode material [J]. *Nano Energy*, 2018, 48: 81-92.
- [8] Xu C, Liao J, Wang R, et al. MoO<sub>3</sub>@Ni nanowire array hierarchical anode for high capacity and superior longevity all-metal-oxide asymmetric supercapacitors [J]. *RSC Advances*, 2016, 6 (111): 110112-110119.
- [9] Liao J, Wang X, Wang Y, et al. Lavender-like cobalt hydroxide nanoflakes deposited on nickel nanowire arrays for high-performance supercapacitors [J]. *RSC Advances*, 2018, 8 (31): 17263-17271.
- [10] Cook J B, Kim H S, Lin T C, et al. Pseudocapacitive charge storage in thick composite MoS<sub>2</sub> nanocrystal-based electrodes [J]. *Advanced Energy Materials*, 2017, 7 (2): 1601283.
- [11] Wu Q, Xu Y, Yao Z, et al. Supercapacitors based on flexible graphene/polyaniline nanofiber composite films [J]. *ACS nano*, 2010, 4 (4): 1963-1970.
- [12] Zhou C, Zhang Y, Li Y, et al. Construction of high-capacitance 3D CoO@polypyrrole nanowire array electrode for aqueous asymmetric supercapacitor [J]. *Nano Letters*, 2013, 13 (5): 2078-85.
- [13] Pang H, Li X, Zhao Q, et al. One-pot synthesis of heterogeneous Co<sub>3</sub>O<sub>4</sub>-nanocube/Co(OH)<sub>2</sub>-nanosheet hybrids for high-performance flexible asymmetric all-solid-state supercapacitors [J]. *Nano Energy*, 2017, 35: 138-145.
- [14] Zhai T, Wan L, Sun S, et al. Phosphate ion functionalized Co<sub>3</sub>O<sub>4</sub> ultrathin nanosheets with greatly improved surface reactivity for high performance pseudocapacitors [J]. *Advanced Materials*, 2017, 29 (7).
- [15] Simon P, Gogotsi Y. Materials for electrochemical capacitors [J]. *Nature Materials*, 2008, 7 (11): 845-54.
- [16] Raza W, Ali F, Raza N, et al. Recent advancements in supercapacitor technology [J]. *Nano Energy*, 2018, 52: 441-473.
- [17] Kawamori M, Asai T, Shirai Y, et al. Three-dimensional nanoelectrode by metal nanowire nonwoven clothes [J]. *Nano Letters*, 2014, 14 (4): 1932-7.
- [18] Xu C, Liao J, Yang C, et al. An ultrafast, high capacity and superior longevity Ni/Zn battery constructed on nickel nanowire array film [J]. *Nano Energy*, 2016, 30: 900-908.
- [19] Yuan C, Yang L, Hou L, et al. Flexible hybrid paper made of monolayer Co<sub>3</sub>O<sub>4</sub> microsphere arrays on rGO/CNTs and their

- application in electrochemical capacitors [J]. *Advanced Functional Materials*, 2012, 22 (12): 2560-2566.
- [20] Qi J, Mao J, Zhang A, et al. Facile synthesis of mesoporous ZnCo<sub>2</sub>O<sub>4</sub> nanosheet arrays grown on rGO as binder-free electrode for high-performance asymmetric supercapacitor [J]. *Journal of Materials Science*, 2018, 53 (23): 16074-16085.
- [21] Sulaiman Y, Azmi M K S, Mohd Abdah M A A, et al. One step electrodeposition of poly-(3,4-ethylenedioxythiophene)/graphene oxide/cobalt oxide ternary nanocomposite for high performance supercapacitor [J]. *Electrochimica Acta*, 2017, 253: 581-588.
- [22] Wang G, Zhang L, Zhang J. A review of electrode materials for electrochemical supercapacitors [J]. *Chemical Society Reviews*, 2012, 41 (2): 797-828.
- [23] Liao J, Zou P, Su S, et al. Hierarchical nickel nanowire@NiCo<sub>2</sub>S<sub>4</sub> nanowhisker composite arrays with a test-tube-brush-like structure for high-performance supercapacitors [J]. *Journal of Materials Chemistry A*, 2018, 6 (31): 15284-15293.
- [24] Zou P, Li J, Zhang Y, et al. Magnetic-field-induced rapid synthesis of defect-enriched Ni-Co nanowire membrane as highly efficient hydrogen evolution electrocatalyst [J]. *Nano Energy*, 2018, 51: 349-357.
- [25] Zou P, Chiang S W, Li J, et al. Ni@Li<sub>2</sub>O co-axial nanowire based reticular anode: Tuning electric field distribution for homogeneous lithium deposition [J]. *Energy Storage Materials*, 2018.
- [26] Xing L, Dong Y, Hu F, et al. Co<sub>3</sub>O<sub>4</sub> nanowire@NiO nanosheet arrays for high performance asymmetric supercapacitors [J]. *Dalton Transactions*, 2018, 47 (16): 5687-5694.
- [27] Yang Q, Lu Z, Li T, et al. Hierarchical construction of core-shell metal oxide nanoarrays with ultrahigh areal capacitance [J]. *Nano Energy*, 2014, 7: 170-178.
- [28] Noh M, Kwon Y, Lee H, et al. Amorphous carbon-coated tin anode material for lithium secondary battery [J]. *Chemistry of Materials*, 2005, 17: 1926-1929.
- [29] Zuo Y, Ni J, Song J, et al. Synthesis of Co<sub>3</sub>O<sub>4</sub>/NiO nanofilms and their enhanced electrochemical performance for supercapacitor application [J]. *Applied Surface Science*, 2016, 370: 528-535.
- [30] Wan C, Jiao Y, Li J. Multilayer core-shell structured composite paper electrode consisting of copper, cuprous oxide and graphite assembled on cellulose fibers for asymmetric supercapacitors [J]. *Journal of Power Sources*, 2017, 361: 122-132.
- [31] Yao H, Zhang F, Zhang G, et al. A new hexacyanoferrate nanosheet array converted from copper oxide as a high-performance binder-free energy storage electrode [J]. *Electrochimica Acta*, 2019, 294: 286-296.
- [32] Bai Y, Liu R, Li E, et al. Graphene/carbon nanotube/bacterial cellulose assisted supporting for polypyrrole towards flexible supercapacitor applications [J]. *Journal of Alloys and Compounds*, 2019, 777: 524-530.